CHEMISTRY
A EUROPEAN JOURNAL

DOI: 10.1002/chem.200903535

Compression of Self-Assembled Nano-Objects: 2D/3D Transitions in Films of (Perfluoroalkyl)Alkanes—Persistence of an Organized Array of Surface Micelles

Caroline de Gracia Lux,[a] Jean-Louis Gallani,[b] Gilles Waton,[a] and Marie Pierre Krafft*[a]

Abstract: Understanding and controlling the molecular organization of amphiphilic molecules at interfaces is essential for materials and biological sciences. When spread on water, the model amphiphiles constituted by $C_nF_{2n+1}C_mH_{2m+1}$ (*FnHm*) diblocks spontaneously self-assemble into surface hemimicelles. Therefore, compression of monolayers of *FnHm* diblocks is actually a compression of nanometric objects. Langmuir films of *F*8*H*16, *F*8*H*18, *F*8*H*20, and *F*10*H*16 can actually be compressed far beyond the "collapse" of their monolayers at ~30 Å^2. For molecular areas *A* between 30 and 10 Å^2, a partially reversible, 2D/3D transition occurs between a monolayer of surface micelles and a multilayer that coexist on a large plateau. For $A < 10$ Å^2, surface pressure increases again, reaching up to ~48 mN m^{-1} before the film eventually collapses. Brewster angle microscopy and AFM indicate a several-fold increase in film thickness when scanning through the 2D/3D coexistence plateau. Compression beyond the plateau leads to a further increase in film thickness and, eventually, to film disruption. Reversibility was assessed by using compression–expansion cycles. AFM of *F*8*H*20 films shows that the initial monolayer of micelles is progressively covered by one (and eventually two) bilayers, which leads to a hitherto unknown organized composite arrangement. Compression of films of the more rigid *F*10*H*16 results in crystalline-like inflorescences. For both diblocks, a hexagonal array of surface micelles is consistently seen, even when the 3D structures eventually disrupt, which means that this monolayer persists throughout the compression experiments. Two examples of pressure-driven transformations of films of self-assembled objects are thus provided. These observations further illustrate the powerful self-assembling capacity of perfluoroalkyl chains.

Keywords: fluorocarbon/hydrocarbon diblocks · Langmuir–Blodgett films · micelles · nanostructures · self-assembly

Introduction

The formation of monolayers, bilayer membranes, and eventually of living cells relies on the self-assembly of amphiphilic molecules. More generally, amphiphilic molecules provide a diversity of organized self-assembled interfaces and objects. This can be achieved by implementing a variety of weak intermolecular interactions. Highly fluorinated materials provide specific interactions, including "halogen bonding",[1,2] and "super" hydrophobic forces[3–6] that can, for example, be used instead of hydrogen bonds in both materials science (e.g., crystal engineering, liquid crystals, magnetic and conducting materials)[1] and bioengineering (e.g., noncanonic protein and nucleic acid pairing).[7]

Perfluoroalkyl (*F*-alkyl) chains have been instrumental in molecular interfacial film stabilization[8] and for inducing

[a] C. de Gracia Lux, Dr. G. Waton, Dr. M. P. Krafft
Systèmes Organisés Fluorés à Finalités Thérapeutiques (SOFFT)
Université de Strasbourg
Institut Charles Sadron (CNRS)
23 rue du Loess, 67034 Strasbourg Cedex 2 (France)
Fax: (+33) 388-41-4099
E-mail: krafft@ics.u-strasbg.fr

[b] Dr. J.-L. Gallani
Département des Matériaux Organiques (DMO)
Université de Strasbourg
Institute of Physics and Chemistry of Materials of Strasbourg (IPCMS)
23 rue du Loess, 67034 Strasbourg Cedex 2 (France)

Supporting information for this article is available on the WWW under http://dx.doi.org/10.1002/chem.200903535.

nanocompartmentalization in self-assemblies.[3,6,9–11] Due to the lipophobic character of *F*-alkyl chains, fluorocarbon/hydrocarbon diblocks ($C_nF_{2n+1}C_mH_{2m+1}$, *FnHm*) display some amphiphilic behavior, despite the absence of a hydrophilic polar head group.[5,6,12,13] A distinctive feature of semifluorinated alkanes is indeed the fact that, although they are apolar in the sense that they do not dissolve in protic solvents, they possess a significant dipole moment that is located at the junction between the two blocks and reflects the strong electron-withdrawing character of the *F*-alkyl chain. These characteristics endow *FnHm* diblocks with specific properties in both the solid (liquid-crystal behavior)[14,15] and liquid states (surface freezing),[16] in solutions (micelle formation in both hydrocarbons and fluorocarbons),[17–19] and at interfaces (formation of stable Langmuir films).[20] *FnHm* diblocks were also found to substantially modify, and usually stabilize, the interfacial films of emulsions,[8] vesicles,[12,21] phospholipid films,[22] and other micro- and nanostructures.[23] Due to a reduced set of interactions at interfaces, *FnHm* diblocks also provide simple models for investigating the self-assembling behavior of amphiphiles.[24]

Langmuir film compression studies constitute an effective approach to the investigation of interfacial films. The Langmuir film behavior of *FnHm* diblocks has been reported in numerous papers from several groups (see in particular refs. [25–37]), and has been critically analyzed in recent reviews.[20,38] These studies generally report surface pressure versus molecular area (π/A) isotherms consisting of a monotonous increase in surface pressure until a collapse pressure is reached. The published collapse pressures attain 20 $mN\,m^{-1}$, depending on the length of the *Fn* and *Hm* segments. The rather low values were taken as reflecting weak amphiphilic character. The reported extrapolated molecular areas A_0 are in the range of 30–35 $Å^2$, and depend only slightly on diblock structure.

A very remarkable feature of *FnHm* diblocks is that they tend to self-assemble spontaneously into surface hemimicelles when spread as Langmuir films on water[39] or deposited on solid supports.[29,30,33,37,40] These surface micelles are highly monodisperse, start forming at very low surface pressures, following a concentration- rather than pressure-dependent mechanism,[41] and, upon compression, organize in regular hexagonal arrays without significant change in micelle size and morphology. The aptitude to form monolayers patterned by surface micelles was shown to originate in the dipole moment of the diblocks[42] and already covers a wide range of compounds ($n=8$–14, $m=14$–20).[30,33] Therefore, Langmuir film studies of these *FnHm* compounds actually concern the compression of arrays of nanometer-sized objects, or supramolecular assemblies, rather than of individual molecules, which provides a unique opportunity for investigating the behavior of films of self-assembled objects. The Langmuir–Blodgett technique is a versatile method that has been widely used to organize nanoscale materials of different morphologies and sizes, including nanoparticles, nanorods, nanowires, carbon nanotubes,[43] and dendrimers.[44] To our knowledge, however, there is no report of the compression of self-assembled nano-objects, except those on surface micelles of *FnHm* diblocks.

The collapse of monolayers of amphiphiles upon compression, although it has been extensively investigated,[45–48] is still poorly understood, even in the case of the widely documented phospholipid films.[49] A recent paper focuses on diblock film behavior immediately before reaching monolayer collapse,[50] and concludes that the nucleation–growth–collision model[46] applies to the behavior of the films of certain diblocks when reaching that collapse; the existence of surface micelles is, however, not taken into account. An interesting recent paper reports the reversible aggregation *after* collapse of rigid bolaamphiphiles fitted with *F*-alkyl chains; however, these compounds also had highly hydrophilic polar head groups, and hence a very different set of interactions.[51]

Herein, we focus primarily on the fate of the self-assembled surface micelles of *FnHm* diblocks when compressed at and beyond monolayer collapse, and evaluate to what extent these structures and their 2D arrangement resist compression and/or reorganize to form self-assemblies different from the initially formed ones. By doing so, we address the question of the compression of self-assembled objects at interfaces. We also explore the behavior of nonpolar interfacial films at pressures beyond the "collapse" of the initially formed monolayer of hemimicelles, and investigate multilayer film formation, 2D/3D film coexistence and reversibility, and final film disruption. The films were further analyzed by Brewster angle microscopy (BAM) at the air/water interface and atomic force microscopy (AFM) after transfer onto silicon wafers.

The diblocks investigated were *F*8*Hm* ($m=16$, 18, and 20) and *F*10*H*16. The longer *Hm* chains were chosen to avoid possible interference with liquid-crystalline phase formation,[14,15] which is only found for diblocks with $m\leq12$,[38] and also because the Langmuir monolayers of these diblocks have proved to be highly stable.

Results

Compression of *FnHm* diblocks revisited

Isotherm characteristics: The surface pressure/area per molecule (π/A) compression isotherms of diblocks *F*8*H*16, *F*8*H*18, *F*8*H*20, and *F*10*H*16 at 15 °C are collected in Figure 1. The isotherms all comprise a first increase in surface pressure that occurs at extrapolated areas A_0 of 32–34 $Å^2$, with a collapse at $\pi_c^1=10$, 14, 16, and 17 $mN\,m^{-1}$, respectively, close to the values given in the literature. The value of A_0 is close to the cross section of an *F*-alkyl chain (~29 $Å^2$).[38] This sequence of events, from the onset of pressure increase until the above, previously identified "collapse", will be designated as the first regime of compression.

It can be seen in Figure 1 that the films can sustain further compression, far beyond the previously documented collapse at ~30 $Å^2$. The surface pressure then remains essential-

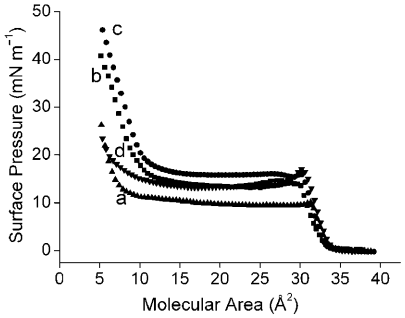

Figure 1. Surface pressure (π)/molecular area (A) isotherms of a) *F8H16*, b) *F8H18*, c) *F8H20*, and d) *F10H16* diblocks (compression speed 5 cm^2 min^{-1}; temperature 15 °C); 50 μL of a 2 mmol L^{-1} *FnHm* solution were spread.

ly constant over a large plateau of molecular area, until the latter reaches ~10 Å^2. This value means that only one third of the molecules are now in contact with the surface of water, thus indicating growth in the third dimension. The collapse at ~30 Å^2 clearly represents a reorganization of the film's structure rather than the usual dissolution or erratic disruption of the film. The plateau indicates that the 3D structures coexist with the monolayer of surface micelles. At the end of the plateau the surface pressure increases sharply again. For *F10H16*, the second pressure rise is much smoother than that for the *F8Hm* compounds; it starts well before A reaches 10 Å^2, and the threefold decrease in molecular area is less obvious. The events from 30 Å^2 on will be designated as the second compression regime.

The pressures at which the films "collapse" for the second time could actually not be determined precisely, as this event takes place at molecular area values that are lower than the lowest area measurable on the trough (when the barriers come into contact). The maximum attainable values (π_{max}) are given in Table 1. Increasing the amount of diblock deposited on the surface allows higher surface pressures to be reached, and hence a more precise investigation of the isotherms at smaller molecular areas and a closer approach to the second collapse. Thus, for example, spreading 50 μL of a 4 mmol L^{-1} solution of *F8H16* at 25 °C, instead of 50 μL of a 2 mmol L^{-1} solution, allows the pressure to rise above 40 mN m^{-1}, instead of 12 mN m^{-1} (Figure 2).

Influence of temperature: The isotherms measured for *F8H16*, *F8H18*, *F8H20*, and *F10H16* at 15, 25, and 35 °C (Figure 3) show that the temperature affects the isotherms in both compression regimes. For all four compounds, the first collapse pressure, as well as the pressure on the coexistence plateau, increases as the temperature decreases (Table 1).

The isothermal compressibility coefficients, C_{s1} and C_{s2}, of the *FnHm* films were calculated at 15, 25, and 35 °C for the two compression regimes, as well as the corresponding compressional moduli (the reciprocal quantity of C_s), C_{s1}^{-1} and C_{s2}^{-1} (see Table 1 in the Supporting Information). For *F10H16*, the C_{s1} values (5.7 to 6.5×10^{-3} mN m^{-1}) do not

Table 1. Surface pressure on the 2D/3D coexistence plateau (π_{pl}), surface pressure at "collapse" in the first regime (π_c^1), maximal surface pressure reachable in the second regime (π_{max}^2), and extrapolated molecular areas (A_0^1 and A_0^2) for the two compression regimes of the *FnHm* diblocks. Three temperatures were investigated: 15, 25, and 35 °C; 50 μL of a 2 mmol L^{-1} *FnHm* solution were spread, unless otherwise specified.

FnHm	Temperature	Plateau	First regime of compression		Second regime of compression	
	[°C]	π_{pl}[a] [mN m^{-1}]	π_c^1 [mN m^{-1}]	A_0^1 [Å^2]	π_{max}^2 [mN m^{-1}]	A_0^2 [Å^2]
	15	10	10	33	27	11
F8H16	25[b]	8	9	33	21	8
	35[c]	7	8	32	43	6
	15	14	14	33	41	12
F8H18	25	12	12	33	39	11
	35	7	8	34	19	9
	15	16	16	33	48	13
F8H20	25	14	14	33	42	13
	35	10	9	34	36	11
	15	13	17	34	25	12
F10H16	25[b]	11	15	34	30	9
	35	10	10	33	22	10

[a] Surface pressure π_{pl} at ~20 Å^2, that is, in the middle of the plateau. [b] 60 μL of a 2×10^{-3} mol L^{-1} solution was spread. [c] 50 μL of a 4×10^{-3} mol L^{-1} solution was spread.

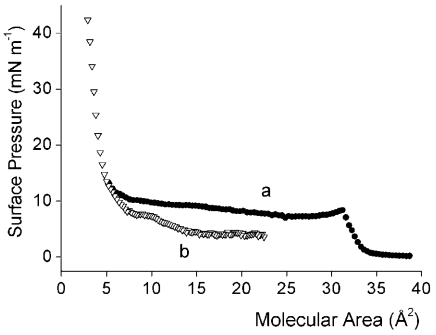

Figure 2. Influence of the amount of *F8H16* spread on the surface of water at 25 °C: a) 50 μL of a 2 mmol L^{-1} solution (●), and b) 50 μL of a 4 mmol L^{-1} solution (▽).

vary significantly with temperature, and are in line with those previously reported. C_{s1}^{-1} values range from 154 to 175 mN m^{-1}, thus indicating that the *F10H16* monolayers are in a liquid condensed state in the range of temperatures investigated. In the second regime, the compressional moduli C_{s2}^{-1} of *F10H16* are much lower than those in the first regime (~20–30 mN m^{-1}) at all temperatures. The meaning of these values is less straightforward as they relate to a multilayer. For the *F8Hm* series, the C_{s1}^{-1} values decrease strongly at 35 °C, and all the more when *Hm* is shorter.

Isotherm reversibility: To determine whether the diblock films would expand again after compression in the two regimes, several increasingly high target pressures were chosen and, in each case, two compression–expansion cycles were performed for each diblock. These experiments also provide an assessment of film stability.

In a first series of experiments, the diblocks were compressed below π_c^1 at 25 °C (Figure 4). It is seen that the iso-

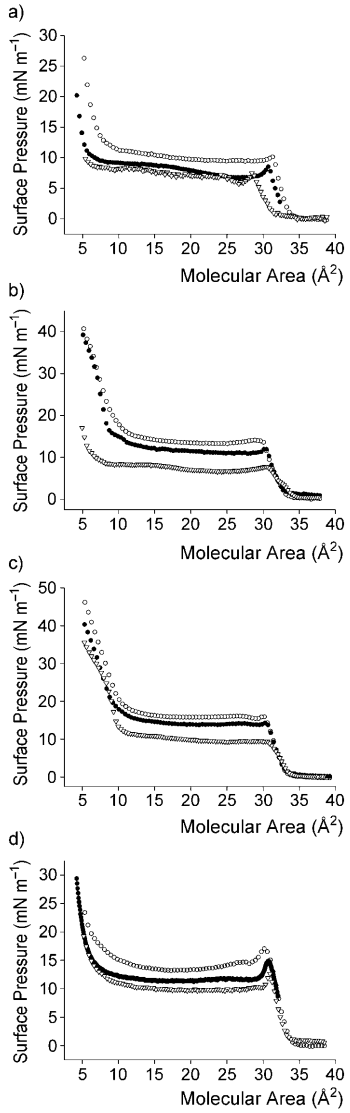

Figure 3. Influence of temperature on films of a) *F8H16*, b) *F8H18*, c) *F8H20*, and d) *F10H16* (compression speed 5 cm^2 min^{-1}). The amounts of *FnHm* spread are given in Table 1 (○: 15 °C, ●: 25 °C, ▽: 35 °C).

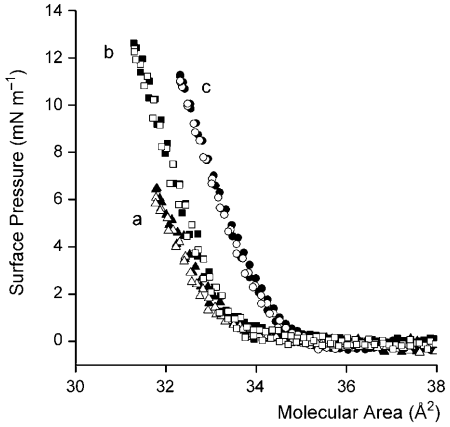

Figure 4. Compression–expansion isotherms π/A of a) *F8H16*, b) *F8H20*, and c) *F10H16* diblocks. The diblocks are compressed below π_c^1 and subsequently re-expanded (compression speed 5 cm^2 min^{-1}; temperature 25 °C). Two compression–expansion cycles (first cycle: solid symbols, second cycle: empty symbols) are performed for each diblock. The isotherms of *F8H18* fall in between curves a and b and are omitted for clarity. 50 μL of a 2 mmol L^{-1} *FnHm* solution were spread.

therms were fully reversible, without hysteresis, during these compression–expansion cycles, which indicates that below the first collapse the monolayers of *FnHm* diblock hemimicelles re-expand on the surface without loss of material.

In a second series of experiments, the diblock films were compressed beyond the first collapse, approximately until the middle of the coexistence plateau (i.e., up to ~8, ~11, ~14, and ~13 mN m^{-1}, with targeted molecular areas of ~17, 16, 16, and 20 Å^2, for *F8H16*, *F8H18*, *F8H20*, and *F10H16*, respectively). Figure 5 a_1, b_1, c_1, and d_1 show that the diblocks re-expand on the surface without loss of material, but definite hysteresis is now seen during the compression–expansion cycles.

The third series of compressions–expansions was achieved in the second pressure increase after the plateau. *F8H18*, *F8H20*, and *F10H16* were compressed up to ~25 mN m^{-1} (Figure 5 b_2, c_2, and d_2). In these cases the films did not re-expand totally. The loss of amphiphiles is substantial to moderate (34, 9, and ~14% for *F8H18*, *F8H20*, and *F10H16*, respectively). Because the maximal pressure that could be reached at 25 °C for *F8H16* molecules was only ~13 mN m^{-1} (Figure 5 a_2), the respreading ability of *F8H16* was also tested at 15 °C. Under these conditions, the maximal surface pressure was about 25 mN m^{-1} (Figure 5 a_3), and ~14% of the molecules were lost after the first cycle.

Compressing the films at pressures larger than 25 mN m^{-1} resulted in greater loss of material. For example, at 40 mN m^{-1}, a pressure that could be attained for *F8H20* without spreading a larger amount of material (50 μL of a 2 mmol L^{-1} solution), 71% of the molecules were lost after the first cycle.

BAM of *FnHm* diblock films on water: Continuous BAM monitoring was carried out for films of *F8H20* and *F10H16* throughout the course of the two compression regimes. The quality of the images allowed dependable analysis of the variation of film height upon compression. An interesting feature of the diblock films investigated is that the molecules stand on average perpendicular to the surface of water in the initial monolayer of surface micelles, and it can reasonably be supposed that this remains the case throughout the compression experiments. Thus, one of the inherent biases of BAM, namely that the refraction index of an amphiphilic molecule varies as its orientation changes upon compression, which can affect thickness values, is largely eliminated.

The compression–expansion experiments were conducted with *F8H20* between molecular areas of 33 and 8 Å^2 near and beyond the first collapse (Figure 6). This range of A values (allowed for an amount of 60 μL of a 2 mmol L^{-1} solution) comprises the first increase in pressure, starting from ~1.5 mN m^{-1}, the coexistence plateau, and a portion of the

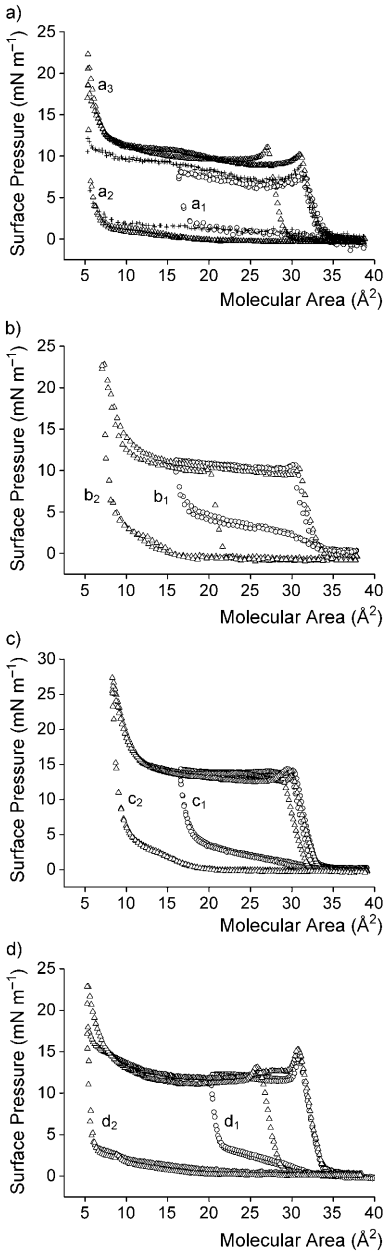

Figure 5. Two successive compression–expansion cycles measured for a) *F8H16*, b) *F8H18*, c) *F8H20*, and d) *F10H16* films (compression speed 5 cm^2 min^{-1}, temperature 25 °C unless otherwise stated). The films were compressed in different stages: a_1) up to 8 mN m^{-1}, 17 Å^2; a_2) up to 13 mN m^{-1}, 5 Å^2; a_3) at 15 °C, up to 23 mN m^{-1}, 5 Å^2; b_1) up to ~11 mN m^{-1}, 16 Å^2; b_2) up to 23 mN m^{-1}, 7 Å^2; c_1) up to 14 mN m^{-1}, 16 Å^2; c_2) up to 27 mN m^{-1}, 8 Å^2; d_1) up to 13 mN m^{-1}, 20 Å^2; and d_2) up to 24 mN m^{-1}, 5 Å^2. 50 μL of a 2 mmol L^{-1} *FnHm* solution were spread, except for *F10H16* (60 μL).

second increase in pressure, up to ~23 mN m^{-1}. Figure 6 exemplifies typical BAM snapshots of an *F8H20* film; the pressures at which the images were taken are indicated on the isotherm of Figure 7.

During the first pressure rise (~30–34 Å^2), a rather uniform light gray phase is seen on the images (Figure 6a, taken at point a in Figure 7). At 30 Å^2, a brighter upper phase appears on top of the monolayer and progressively develops upon compression across the plateau (see, for example, Figure 6b, which corresponds to point b in Figure 7). Upon further compression, a densification of the upper phase is seen. At the end of the coexistence plateau (~11 Å^2, point c in Figure 7), a still brighter upper phase is seen that completely covers the lower phase (Figure 6c). Remarkably, when pressure is further increased (beyond 15 mN m^{-1}; points d and e in Figure 7), cracks appear (Figur-

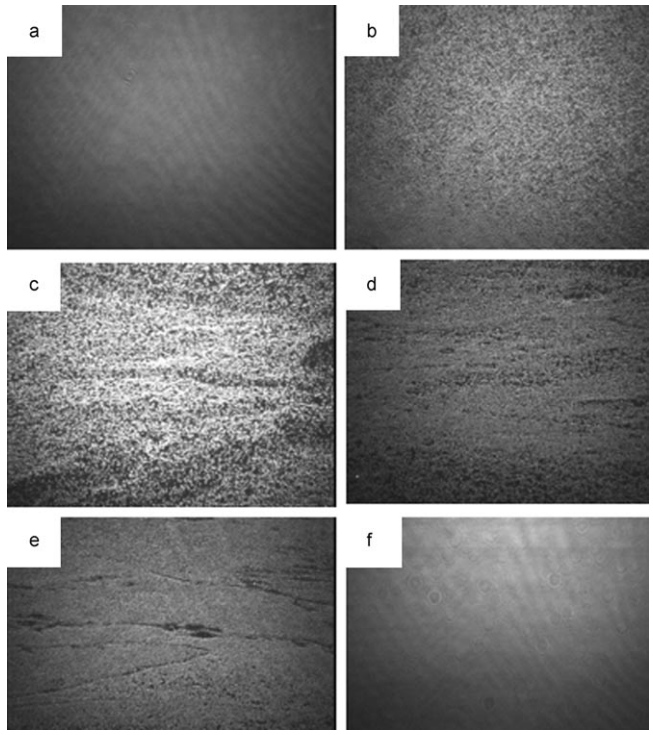

Figure 6. BAM images taken during compression of a film of *F8H20* at the air/water interface. The size of the micrographs is 500×600 μm^2; 60 μL of a 2 mmol L^{-1} diblock solution were spread.

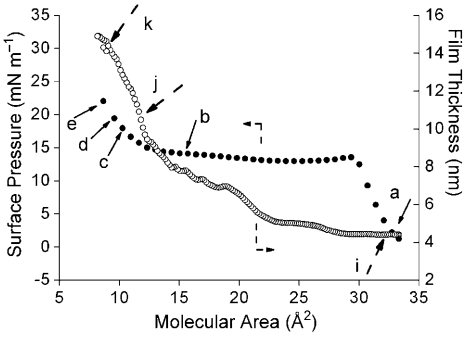

Figure 7. Surface pressure (●) and film thickness (○) as a function of molecular area for films of *F8H20* (60 μL of a 2 mmol L^{-1} diblock solution spread on water). Surface pressures prior to compression were around 1.5 mN m^{-1}. The letters a–e indicate the molecular areas at which the BAM snapshots of Figure 6 were taken, and i–k the film thicknesses at various *A* values (see text).

e 6d, e), followed by the appearance of zones of the initial lower gray phase, which indicates disruption of the upper layers. When the film is allowed to expand again down to ~0 mN m^{-1}, the light gray lower phase of Figure 6a eventually reappears (Figure 6f).

The variation of the thickness of the film of *F*8*H*20 as a function of molecular area is shown in Figure 7, in which the number of molecules deposited at the interface was such that the maximum and minimum reachable molecular areas were ~33 and ~8 Å^2, respectively. Under these conditions, the thickness of the film increases from (4.4 ± 1) to (11.1 ± 2) nm (points i and j in Figure 7) when the pressure increases from a few to ~15 mN m^{-1}. The value of 4.4 nm is close to the length of the fully extended *F*8*H*20 diblock (3.90 nm). The value of 11.1 nm is about three times the height of the initial film. Then, when the pressure further increases from ~15 to ~30 mN m^{-1}, the thickness of the film reaches ~(14.7 ± 1) nm (point k in Figure 7), which corresponds to about four to five times the length of the diblock.

In the case of *F*10*H*16, separate BAM experiments (with increasing amounts of diblocks) were run to investigate the first collapse and the coexistence plateau, to explore the highest reachable surface pressures (during the second pressure increase), and to probe reversibility.

The first compression experiment (Figure 8A) was conducted with *F*10*H*16 between molecular areas of 38 and 8 Å^2, the range of *A* values allowed for the amount (40 μL of a 2 mmol L^{-1} solution) of material deposited (Figure 8Aa–e). At molecular areas approaching the first pressure lift-off (~38 Å^2, point a in Figure 9), *F*10*H*16 forms large domains on the surface of water that have a typical liquid condensed-like aspect, that is, sharp edges and high optical density (Figure 8Aa).

During the first pressure rise (30–34 Å^2), these domains cover the whole observation field, and a uniform light gray phase is seen in the images (Figure 8Ab, which corresponds to point b in Figure 9), which is comparable to that seen for *F*8*H*20 at the low pressures. At 30 Å^2 (the collapse of the monolayer, point c in Figure 9), bright dots start to appear (Figure 8Ac) that reflect punctual increases in film height. Beyond this first collapse, as further compression is applied, these dots become more numerous and larger (Figure 8Ad, point d in Figure 9). An upper layer is observed to develop that progressively covers the initial monolayer (Figure 8Ae, point e in Figure 9).

The second compression experiment (Figure 8B) was devised to explore the higher surface pressures. Therefore, a larger amount of diblock (60 μL instead of 40 μL of the 2 mmol solution) was deposited, which allows a surface pressure of ~30 mN m^{-1} (isotherm indicated by triangles in Figure 9) to be reached. Figure 8Bf (16 mN m^{-1}, 6 Å^2, corresponding to point f in Figure 9) is essentially identical to Figure 8Ae, but further compression results in the appearance of an increasingly dense maze of fiberlike structures (Figure 8Bg: 20 mN m^{-1}, 5 Å^2, point g; and Figure 8Bh: 22 mN m^{-1}, <5 Å^2, point h), which was not seen in any of the BAM images of the *F*8*H*20 films.

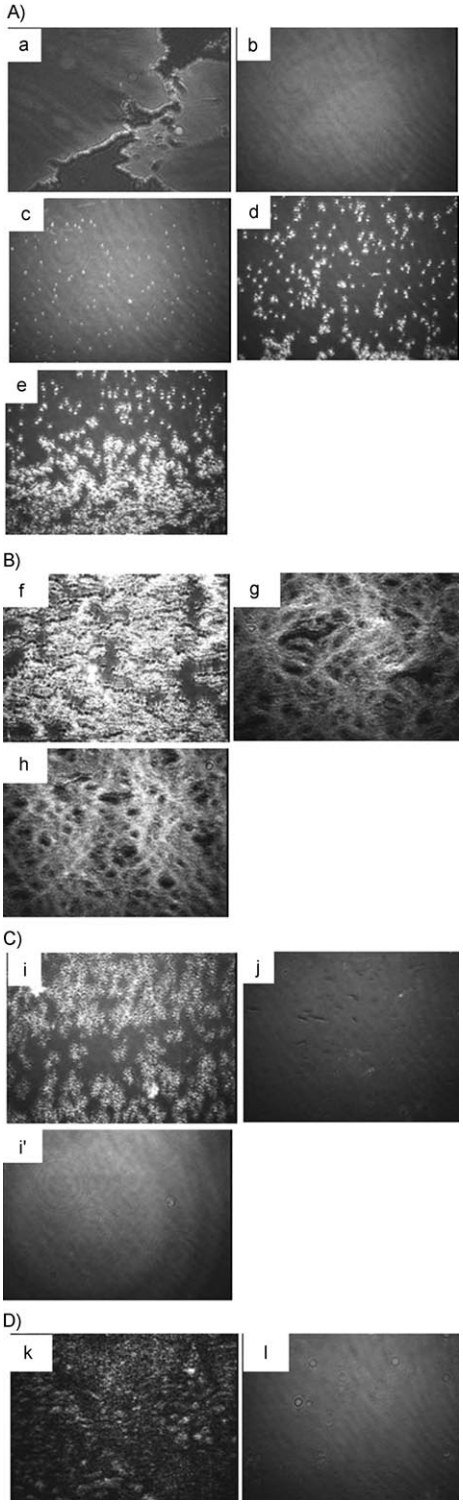

Figure 8. BAM images taken during compression and expansion of a film of *F*10*H*16 at the air/water interface. A) First compression experiment between $A = 38$ and 8 Å^2 (40 μL of a 2 mmol L^{-1} solution). The lowercase letters indicate the molecular areas (shown on the isotherm of Figure 9) at which the selected snapshots were taken. B) Compression of a larger amount of material (60 μL of a 2 mmol L^{-1} solution), which allowed investigation at higher pressures. C, D) Expansions of the films imaged in (A) and (B), respectively. The size of the micrographs is 500 × 600 μm^2.

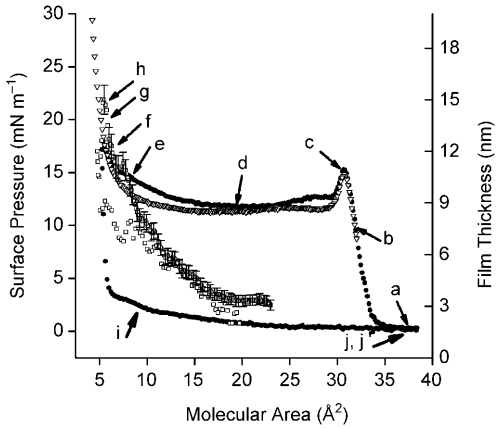

Figure 9. Surface pressure as a function of molecular area for *F*10*H*16 films for two amounts deposited (●: 40 μL, and ▽: 60 μL, of a 2 mmol L^{-1} solution). Average film thickness (□) as a function of molecular area for *F*10*H*16 films (60 μL of a 4 mmol L^{-1} solution deposited). Thin arrows and letters: points at which BAM images were taken during compression (a–h); broad arrows: during expansion (i–j′).

Film expansion experiments were performed starting both at 18 mN m^{-1}, 5 Å, in the first experiment (Figure 8C) and at 30 mN m^{-1}, 4 Å, in the second (Figure 8D). When the film is allowed to re-expand from the end of the plateau ($A = \sim 5$ Å^2 in Figure 9), the upper domains progressively disappear, as seen in Figure 8Ci at 8 Å^2 (point i in Figure 9). Eventually, at ~30 Å^2, the upper domains have completely disappeared and the initial uniform light gray lower phase is seen again (Figure 8Cj and j′; 10 min have elapsed between points j and j′). When expansion is achieved starting from the highest pressures (30 mN m^{-1}), one likewise observes progressive disappearance of the upper maze (Figure 8Dk) until the initial light gray lower phase re-appears (Figure 8Dl). Both expansion experiments establish the reversibility of the 2D/3D transitions.

The variation of the thickness of *F*10*H*20 films is shown in Figure 9. The initial value of the film thickness is ~(3.4 ± 1) nm, which is in good agreement with the length of the fully extended *F*10*H*16 diblock (3.66 nm). At the end of the 2D/3D coexistence plateau (point e in Figure 9), the film thickness is ~(9 ± 2) nm, the pressure remaining essentially constant at ~12 mN m^{-1}. As found for *F*8*H*20, the thickness of the film at the end of the plateau is about three times its initial thickness. It is noteworthy that the thickness of the film after its expansion is 3 nm, which is similar to its value before compression. Further compression (see Figure 9, squares) causes the thickness of the *F*10*H*16 film to increase well above 15 nm, the limiting value obtained for *F*8*H*20 films.

AFM of transferred *FnHm* diblock films: It has previously been established that *FnHm* diblocks self-assemble into regular arrays of surface micelles when spread as monolayers at the air/water interface,[39] or when deposited on a solid surface using Langmuir–Blodgett[30] or spin-coating techniques.[33] AFM monitoring was essential for achieving the prime objective of this work, namely to investigate the 3D structures that build up upon compression of the monolayer of surface hemimicelles beyond its collapse. *F*8*H*20 was selected for this study because it allows compression at the highest pressure values.

When transferred during the first regime of compression, that is, at $\pi < 14$ mN m^{-1} at 25 °C, all the films of *F*8*H*20 exhibit the expected characteristic pattern of surface hemimicelles, each with a diameter of ~35 nm and a height of ~3 nm (Figure 10). As long as the surface pressure is low, the number of elongated micelles is limited, in agreement with the literature.[30]

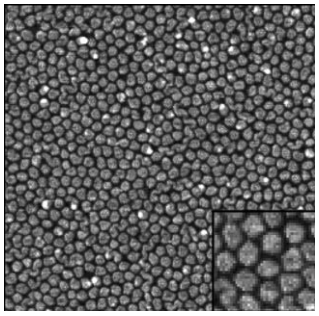

Figure 10. AFM image (1×1 μm^2) of a film of *F*8*H*20 compressed at 3 mN m^{-1} and transferred onto a silicon wafer. Inset: Magnification of the hexagonal array of surface micelles.

Figure 11 shows AFM images taken beyond the collapse of the monolayer, at the beginning of the 2D/3D coexistence plateau, for *F*8*H*20 films transferred onto a silicon wafer at 25 °C. At the beginning of the plateau (~14 mN m^{-1}, ~27 Å^2), the carpet of surface micelles is still observed (Figure 11a). The micelles are, however, packed more closely than in Figure 10, and are somewhat deformed from circular to faceted (inset of Figure 11a′$_h$); the number of elongated micelles has increased, as reported in ref. [30]. The new observation is that some higher aggregates are now seen, which were not present at lower surface pressures. The large-field images display many such aggregates (Figure 11a$_h$). The height of the upper aggregates above the carpet of hemimicelles (as determined on 20 separate objects) is ~(6 ± 1) nm (the height of the hemimicelles remaining (3 ± 1) nm). A first indication that the upper aggregate domains lie on top of the monolayer of hemimicelles is, for example, provided by Figure 12a′$_p$, in which partially covered micelles can be seen under the rim of these domains.

When the films are transferred at a molecular area that corresponds to about the middle of the coexistence plateau, the upper aggregates form large, micrometer-sized domains. The profiles show that their height remains essentially constant (~6 nm) and that, in spite of their rugged aspect, the rugosity of their surface is low (less than 1 nm, about the precision of the AFM *z* measurements; Figure 12). The surface presents irregular circumvolutions. It is seen in Figure 12a$_h$ that the upper aggregates do not consist of layers of

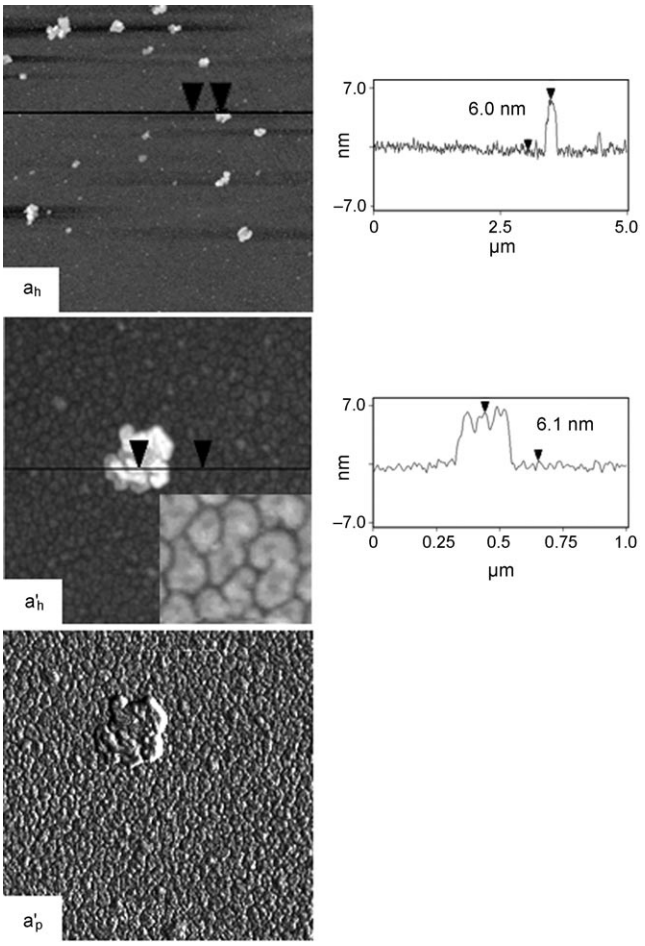

Figure 11. AFM images: a_h) $5\times5\ \mu m^2$ and, at a larger scale, a'_h, a'_p) $1\times1\ \mu m^2$, of a film of *F8H20* diblocks after transfer onto silicon wafers at the beginning of the 2D/3D coexistence plateau (~14 mN m^{-1}, 27 Å^2); the inset in (a'_h) shows a magnification of the carpet of surface micelles. The indices (h) and (p) refer to the height and phase images, respectively. To the right are the corresponding AFM height profiles taken between the two arrowheads shown in the corresponding AFM images.

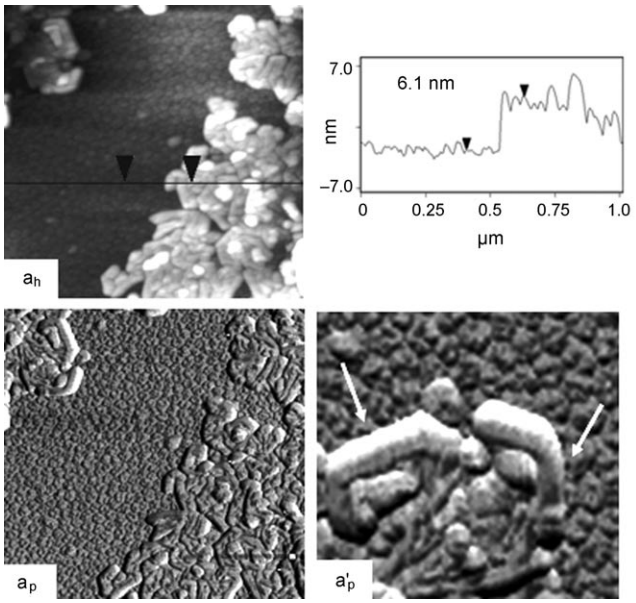

Figure 12. a) AFM images ($1\times1\ \mu m^2$) of a film of *F8H20* diblocks after transfer onto silicon wafers in the middle of the coexistence plateau (at ~14 mN m^{-1}, 20 Å^2). The indices (h) and (p) refer to the height and phase images, respectively. To the right is the height profile taken between the two arrowheads shown in image (a_h). White arrows in (a'_p) indicate examples of hemimicelles partially covered by a protruding upper domain.

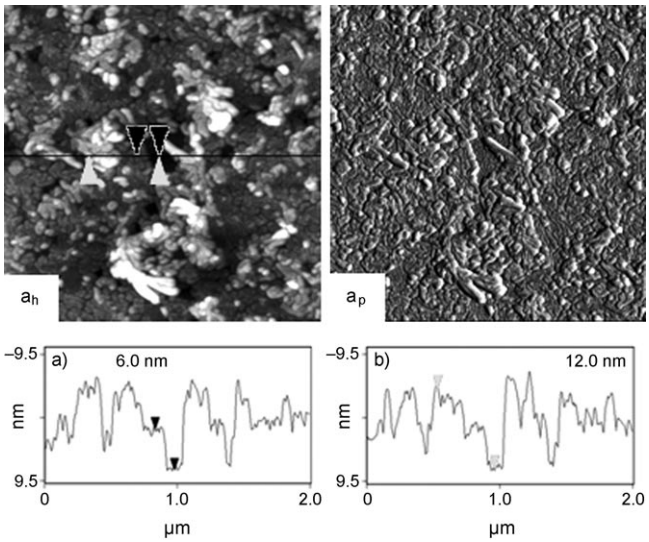

Figure 13. Height (a_h) and phase (a_p) AFM images ($2\times2\ \mu m^2$) of a film of *F8H20* diblocks after transfer onto silicon wafers at a pressure of 25 mN m^{-1}. Under the images are the corresponding AFM profiles measured between the two marks shown in the height image: a) black and b) white arrowheads.

surface micelles, which means that the diblocks have been rearranged in a different type of assembly.

At the end of the plateau, the upper domains cover almost completely the surface of the film, thus forming an essentially continuous layer. However, even before the film of micelles is entirely covered by the 6-nm-high upper layer, it is seen that the 3D phase begins to further increase in height at certain spots. At 25 mN m^{-1}, that is, in the second increase of surface pressure, this additional level of domains (height above the monolayer of micelles: ~12 nm) develops that coexists with the previous 6 nm one (Figure 13).

At 35 mN m^{-1}, the upper phase of *F8H20* becomes still higher in some spots (from ~20 up to 80 nm, see arrows in Figure 14 a_h) and becomes significantly more chaotic. This suggests that the upper phase undergoes general disruption with some protruding stacking of film fragments as part of its collapse process. Most interestingly, the lower monolayer of hemimicelles can be seen again in some areas, which supports the notion that disruption does not affect this monolayer. In particular, the diameter of the surface micelles is essentially unchanged. Instead of the areas of nude wafer usually seen when a Langmuir film collapses, the carpet of hemimicelles (3 nm in height) is again clearly and consistently visible.

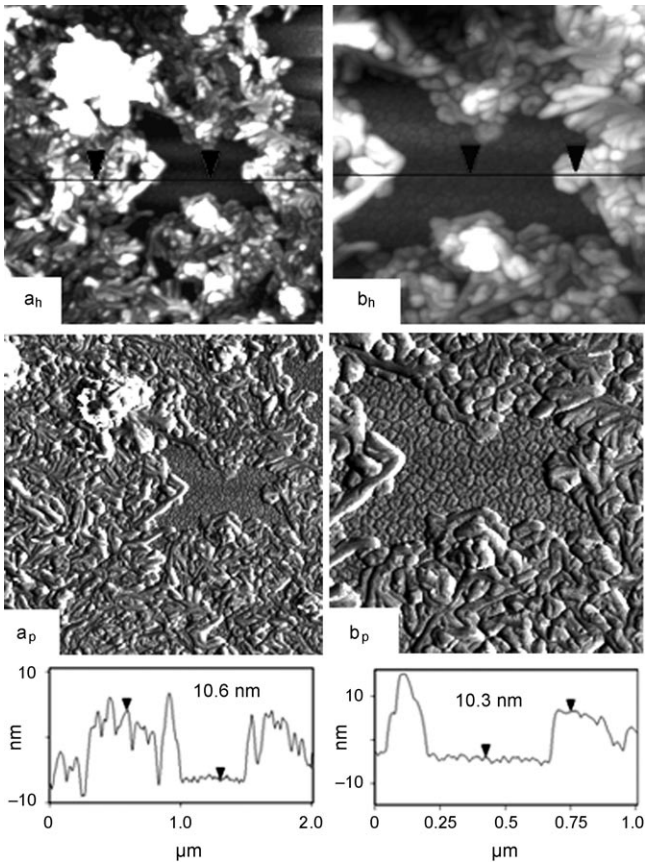

Figure 14. Height (top) and phase (bottom) AFM images (a: 2×2, b: 1×1 μm^2) of a film of *F*8*H*20 diblocks after transfer onto silicon wafers at a pressure of 35 mN m^{-1}. The white arrows in (a_h) indicate higher aggregates (up to 80 nm). Under the images are the corresponding AFM height profiles taken between the two arrowheads in each height image.

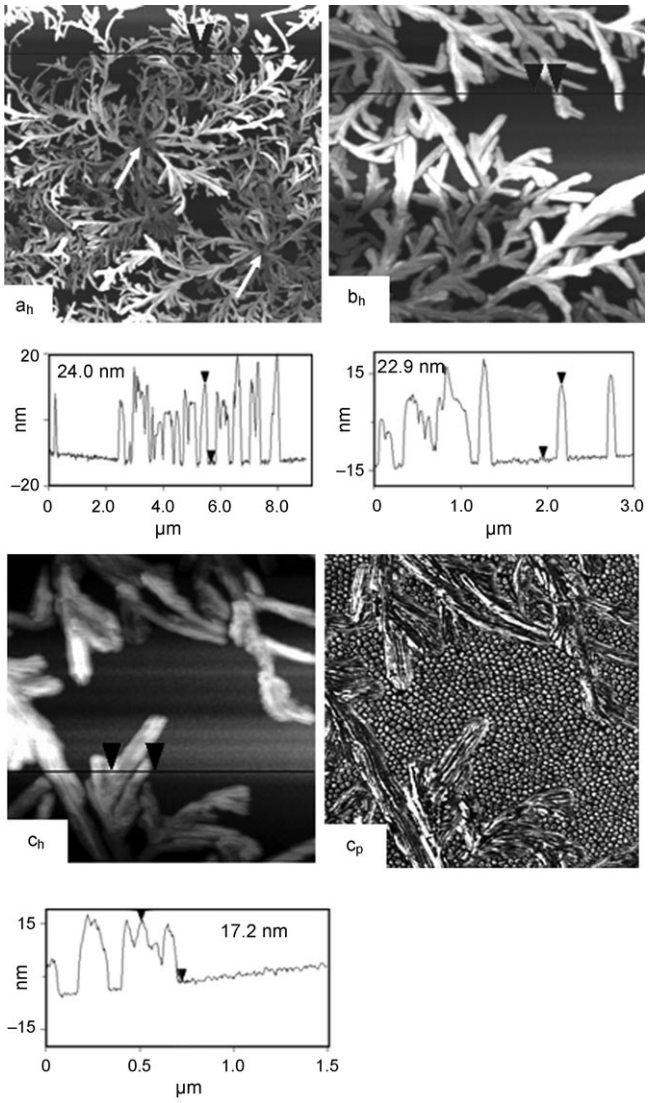

Figure 15. Height AFM images (a_h: 12×12, b_h: 3×3, c_h: 1.5×1.5 μm^2) of a film of *F*10*H*16 diblocks after transfer onto silicon wafers at a pressure of 12 mN m^{-1} ($A \approx 10$ Å^2). c_p) Phase image corresponding to (c_h) (1.5×1.5 μm^2). Under the images are the corresponding AFM height profiles. Typical heights are measured between the two arrowheads shown in each image.

The AFM images of films of *F*10*H*16 (also transferred at 25 °C) are substantially different from those of films of *F*8*H*20. Spectacular images were obtained at the end of the coexistence plateau (at 12 mN m^{-1}, $A \approx 10$ Å^2). In the large-scale image (Figure 15 a_h; 12×12 μm^2), the surface is almost completely covered by well-developed entangled dendritic inflorescences. These structures start developing from precisely identifiable nodes or nuclei (see white arrows in Figure 15 a_h) and have a consistent height of about 20–30 nm (see also the 3×3 μm^2 image, Figure 15 b_h). These dendritic structures have a striated, crystalline aspect (Figure 15 c_h).

Again, a carpet of hemimicelles is consistently seen in the background under the leaflike structures. The AFM phase images show clearly the superimposition of the two types of self-assemblies that coexist in the films (Figure 15 c_p).

Transfer of *F*10*H*16 films at the beginning of the plateau (20–25 Å^2, 12 mN m^{-1}) was attempted. Dendritic structures, comparable to those found at the end of the plateau but smaller in size, were expected. However, AFM experiments (see Figure 1 in the Supporting Information) only revealed the presence of surface micelles, similar in size and morphology to those typically observed in the first regime of compression. It may be that the smaller, not yet entangled, dendritic nuclei are more labile and are eliminated during the transfer.

Discussion

(*F*-alkyl)alkanes constitute a family of simplified model surfactants, devoid of polar head groups.[17,24,38] When spread on water, these compounds spontaneously self-assemble into surface hemimicelles. When reaching the first pressure lift-off recorded on their Langmuir isotherms, their monolayers consist of regular hexagonal arrays of such surface micelles,[29,30,33,39,40] as further confirmed by the AFM studies reported here. Therefore, the present study really concerns

the compression of monolayers of self-assembled objects rather than of independent molecules.

We wanted to determine what happens to this array of surface micelles upon further compression, whether these objects and their arrangement resist compression beyond monolayer collapse, whether they are still present within the film that develops on the 2D/3D coexistence plateau, whether the reorganization that occurs on this plateau is reversible, and to determine the eventual fate of the surface micelles when the multilayer collapses.

Compressing *FnHm* diblocks at the air/water interface—partially reversible 2D/3D structural transformations: This study establishes that the films of surface micelles of the *FnHm* diblocks investigated here are compressible well above their previously reported "collapse" pressure. The compression isotherms of these diblocks all display the remarkable feature of having two successive rises in surface pressure, which leads to two successive collapses with a plateau in between. However, the 3D structures that grow on the plateau differ strongly, depending on the molecular structure of the diblock. Self-assembled hemimicelles are expected to be labile, and therefore prone to reassembly in different ways.

In the case of *F*8*H*20, at the collapse of the initially formed monolayer, a bilayer starts nucleating on top of the surface hemimicelles. This first "collapse" thus corresponds to a 2D/3D transition in which the monolayer of surface micelles experiences the growth of 3D domains the height of which corresponds to a bilayer. This collapse is thus not of the usually encountered type that corresponds to an irreversible disorganization and loss of molecules, but relates to a reorganization of the film from a monolayer to a composite trilayer. During the reorganization process, individual diblock molecules, or hemimicelles, need therefore to be expelled from the surface to form the upper layers. It is expected that, when deprived of their anchorage on water, the hydrocarbon segments will tend to segregate to form an internal core and isolate themselves from the fluorocarbon segments, whereas the latter would extend outwards, thereby initiating the formation of a bilayer. The multilayer (monolayer plus bilayer on top) develops on a large-molecular-area plateau (from ~30 to ~10 Å), without significant change in surface pressure. It is notable that the upper layer is not a second layer of hemimicelles.

At the end of the plateau of the *F*8*H*20 π/A curve, the surface pressure rises again, which means that the bilayer has completely covered the carpet of surface micelles and is being compressed. Still higher surface pressures can be applied (up to 48 mN m^{-1} at 15 °C in the case of *F*8*H*20), which result in the development of a second bilayer on top of the first. The latter may result from buckling and folding of the first bilayer, as established in the case of phospholipids.[49,52] Eventually, further compression leads to the rupture and final "collapse" of the film, at which point fragments of bilayer start piling up in the third dimension, on a scale larger than the molecular scale. At this point, the apparently "indestructible" carpet of surface hemimicelles reappears consistently on the AFM images.

The 2D/3D transition is reversible until the middle of the plateau, approximately. Further compression leads to significant, irreversible loss of molecules, in line with the fact that when the bilayer develops to a large extent on the carpet of surface micelles, it becomes increasingly difficult, or takes more time, for the film to re-expand.

BAM and AFM measurements of the heights of the films made at the different stages of compression are in good agreement. Both methods demonstrate that, starting from an initial height corresponding to the diblock molecules' length, the film reaches a height of about three times this length at the end of the coexistence plateau. Then, the film's height rapidly increases to about five times the molecular length during the second surface pressure increase. The AFM images indicate that the collapse of the bilayer into a double bilayer starts as soon as it is compressed, immediately after the plateau.

The behavior of films of *F*8*H*20 diblocks upon compression is summarized in Figure 16. The diblock chain orientations proposed maximize the favorable *Fn–Fn* chain and *Fn* chain–air interactions, and minimize the unfavorable *Fn–Hm* chain interactions. The orientation of the diblocks in their monolayers has been established by X-ray reflectivity.[26,29] It has also been found for surface-frozen diblock films and Gibbs films.[53,54] The sublayers formed by the *Fn* blocks are expected to be rather rigid and well organized, whereas the *Hm* sublayers are in a liquid state.[38]

The macroscopic behaviors of *F*10*H*16 and *F*8*H*20 are similar, with two pressure increases and a 2D/3D coexistence plateau. However, the nanostructures revealed by AFM are substantially different. Instead of forming a bilayer after the collapse of the monolayer of hemimicelles, the *F*10*H*16 molecules expelled from the water surface form large crystalline-like dendritic structures or inflorescences. The height of these structures is typically ~20–30 nm. The inflorescences were detected only when the transfers on the silicon wafers were achieved at the end of the plateau. At this advanced stage of compression the dendrites have indeed grown enough to entangle and form a network, which may help them withstand transfer onto the wafer. On the other hand, no dendritic structures are detected when the transfer was done at the beginning of the plateau. The only structures seen under the latter conditions are the usual, omnipresent arrays of surface micelles (see Figure 1 in the Supporting Information). At these early compression stages, the dendrites that are most likely formed would still be small and independent, and hence more easily drained off during the transfer or more prone to disappear when compression stress is released during transfer. The fact that the isotherms of *F*10*H*16 are reversible until the middle of the plateau also supports the view that the dendritic nuclei remain small enough over a large range of molecular areas such that they can be reintegrated in the carpet of surface micelles during expansion. The observation of bright dots in the BAM images of *F*10*H*16 (but not for *F*8*H*20) just at the

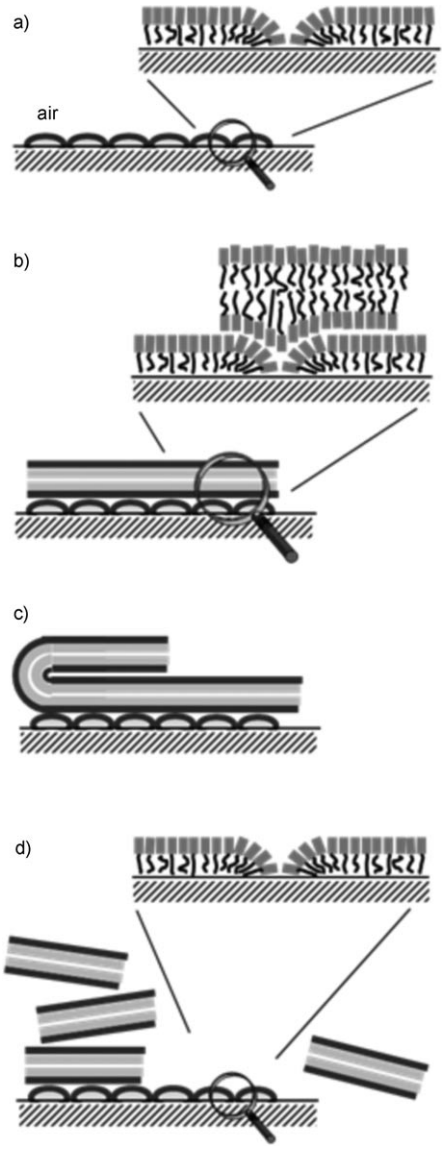

Figure 16. Schematic representation of the behavior of *F*8*H*20 diblock films when compressed at the air/water interface: a) during the first increase in surface pressure; b) at the end of the monolayer/(monolayer + bilayer) coexistence plateau; c) during piling up of a second bilayer during the second pressure rise; and d) at the collapse of this pentalayer, when bilayer fragments start stacking and the monolayer of surface hemimicelles reappears (not to scale).

beginning of the plateau (Figure 8Ac) may be related to the formation of the nuclei. Likewise, the upper bright maze seen at 20 mN m^{-1} ($A \approx 5$ Å^2, Figure 8Bg,h) could be the BAM visualization of the large dendrites seen by AFM after transfer when nearing the end of the plateau. *F*10*H*16 has the highest *F*/*H* ratio among the diblocks investigated; the rigidity of the *F*10 block appears then to take over the diblock behavior. Eventually, the behavior of *F*10*H*16 rejoins that of *F*8*H*20 in that the monolayer of hemimicelles is still visible at the highest attainable pressures.

Persistence of regular arrays of surface hemimicelles as part of composite surface films: The self-assembly of *F*8*H*16 diblocks into surface micelles and the regular organization of the latter on water have previously been established through grazing incidence small-angle X-ray scattering experiments performed directly on the surface of water at surface pressures ranging from 0.5 to 7 mN m^{-1}.[39] These hemimicelles are circular, ~30 nm in diameter, independently of pressure and compression conditions.[41] Their size after transfer onto silicon wafers is very close to that measured on water.[30,39] They were qualified as "sturdy" on the basis that AFM images could be recorded at very small scales without destruction.

A remarkable result of the present study is that a carpet of hemimicelles is observed to remain present throughout all the compression experiments and for all the diblocks investigated: 1) during the first compression regime, they progressively cover the surface of water and are seen on wafers for any chosen pressure (forming a regularly patterned monolayer; e.g., Figure 10); 2) hemimicelles with essentially unchanged shape and size are seen in the AFM images under the rim of the upper bilayer domains formed in the films of *F*8*H*20 during the second compression regime (e.g., Figure 12a$_p'$); 3) they are consistently seen in the background behind the dendritic inflorescences formed by *F*10*H*16 (e.g., Figure 15c$_h$ and 15c$_p$); and 4) they eventually reappear when nearing the second collapse, when the surface film of *F*8*H*20 is disrupted during the second increase in surface pressure. It can be added that the *Fn* chains of the upper bilayer are similar to air in terms of intermolecular interactions,[5] and are not expected to perturb the carpet of micelles significantly.

The unique, composite nature of the films of diblocks, which comprise a highly organized layer of surface micelles topped by 3D structures consisting of a more compressible bilayer or double bilayer, or of crystalline-like inflorescences, constitutes a novel situation. The former system may be viewed as an example of spontaneously formed Langmuir–Blodgett self-assembly.

The present data confirm the outstanding sturdiness of the monolayers of hemimicelles of *FnHm* diblocks, as these micelles appear to withstand both compression episodes without detectable changes in size and morphology (apart from deformations from essentially circular to somewhat hexagonal), which suggests their possible use as templates in bottom-up elaboration of organized arrays of metallic or polymeric nanostructures.

Organizing capacity of semifluorinated alkanes versus "complete" surfactants: The recorded second collapse pressures are unexpectedly high (up to 48 mN m^{-1} at 15 °C for *F*8*H*20) for molecules that have no hydrophilic polar head group (and hence, no possibility of hydrogen-bonding or other interactions stronger than van der Waals), and that are generally considered as being only weakly amphiphilic. *FnHm* diblocks display, however, substantial dipole–dipole interactions.[42] The surface tension reduction potential of *FnHm* di-

blocks has indeed been evaluated to be on the order of 3–5 $mN\,m^{-1}$ only,[24] and is, at any rate, lower than the difference in surface tension between fluorocarbons and hydrocarbons, that is, ~10 $mN\,m^{-1}$.[38] For *F*8*H*20, the surface pressures at which the film eventually "collapses" attain values that are over two times larger than those measured for the first collapse. The former values are comparable to those typically measured for standard (or "complete") surfactants fitted with a hydrophilic polar head group.

The unanticipated observation that the simple "apolar" *FnHm* diblock molecules can form stable and complex organized films on water implies that the parameters that determine film organization and stability are not confined to surface tension, but also include the outstanding capacity for *F*-alkyl chains to promote self-assembly and ordering. In doing so, they convert the compression of layers of molecules into compression of arrays of self-assembled objects. The hydrophobic interactions generated by *F*-alkyl chains provide a powerful driving force, not only for stabilizing monolayers of *FnHm* diblocks at the air/water and air/solid interfaces, but also for driving and stabilizing the formation of composite multilayers and other assemblies at these interfaces.

Conclusion

We have reported a number of unanticipated observations. 1) Monolayers of *FnHm* diblocks can be compressed far beyond their documented "collapse". 2) Rather than dissolution or random disruption, such compression results, in the case of *F*8*H*20, in the building up of one, and eventually two, superimposed bilayers on top of the initially formed monolayer of surface micelles, and, in the case of the stiffer *F*10*H*16, in the development of crystalline-like dendritic inflorescences. 3) A large 2D/3D coexistence plateau exists from ~30 to ~10 $Å^2$, between the monolayer of surface hemimicelles and the above 3D structures. 4) The building up of the 3D film is essentially reversible up to the middle of the plateau. 5) The final (irreversible) "collapse" of the films occurs at remarkably high pressures, comparable to those achieved for films of regular surfactants with polar head groups. 6) A lower monolayer of self-assembled, regularly organized surface hemimicelles is preserved throughout the two compression events, without significant change in size and morphology of the micelles, thus confirming their outstanding sturdiness. 7) The films formed beyond the first collapse are composite in nature, and comprise a bottom layer of organized, compressed self-assembled objects topped, in the case of *F*8*H*20, by one, and eventually a second, less organized bilayer(s) of diblock molecules, and, in the case of *F*10*H*16, by dendritic inflorescences. 8) This article thus provides two examples of pressure-driven transformations between discrete self-assembled objects and different types of assemblies of the same molecule within a surface film. 9) These observations further illustrate the outstanding self-assembling capacity of perfluoroalkyl chains and their capacity to promote the formation of sturdy interfacial films.

Experimental Section

Materials: The diblocks *F*8*H*16, *F*8*H*18, *F*8*H*20, and *F*10*H*16 were synthesized according to ref. [55] and purified by repeated crystallizations from methanol. Chemical purity (>99%) was determined by TLC, NMR spectroscopy, elemental analysis, and MALDI-TOF mass spectrometry. Spreading solutions of *FnHm* (2 or 4 $mmol\,L^{-1}$) were prepared in analytical-grade chloroform (Aldrich). Water was purified with a Millipore system (surface tension: 72.1 $mN\,m^{-1}$ at 20°C; resistivity: 18.2 MΩ cm).

The lengths of the fully extended *FnHm* diblocks were calculated, by using the formula $l = 1.306n + 1.265m + 3.26$ (Å),[15] to be 3.39, 3.65, 3.90, and 3.66 nm for *F*8*H*16, *F*8*H*18, *F*8*H*20, and *F*10*H*16, respectively.

Compression isotherms: Surface pressure versus molecular area (π/A) isotherms were recorded on a Langmuir minitrough (Riegler & Kirstein GmbH, Potsdam, Germany) equipped with two movable barriers. The surface pressure was measured by the Wilhelmy plate method. *FnHm* solution (50 μL, 2 $mmol\,L^{-1}$) was spread on the water surface (unless otherwise specified) and 10 min were allowed for solvent evaporation. The compression speed was kept at 5 $cm^2\,min^{-1}$ for all experiments. The temperature was regulated at ±0.5°C. Each experiment was run at least three times. Experimental errors were ±0.5 $mN\,m^{-1}$ on the surface pressure values, and reproducibility on the molecular area values was ±0.5 $Å^2$. The minimum compressibility values, $C_s = (-1/A_{min})(dA/d\pi)$, were calculated for the two compression regimes (see Table 1 in the Supporting Information). The value of A at collapse and the minimal A value were taken for the A_{min} value, for the first and second increase in surface pressure, respectively.

Langmuir–Blodgett films: The films of diblocks were compressed up to the desired surface pressure and transferred (at constant pressure) onto a silicon wafer, previously treated with piranha solution (concd H_2SO_4 + 30% H_2O_2 3:1), by using the Langmuir–Blodgett technique (one monolayer transferred; lift speed: 1 $mm\,min^{-1}$).

AFM images: The transferred films were analyzed with an atomic force microscope (Multimode AFM, NanoScope IV Controller, Digital Instruments, Santa Barbara, CA) in tapping mode. The cantilever (Olympus) was fitted with a 3–10 nm tip. The resonance frequency was 300 kHz and the spring constant was 40 $mN\,m^{-1}$. At least three different samples were analyzed, and several positions were scanned on the wafer for each sample. The error on measurements along the z axis was estimated at ±0.5 nm.

Brewster angle microscopy: BAM allows observation of monolayers directly at the air/water interface. When a light beam linearly polarized parallel to the plane of incidence hits the air/water interface at an angle of 53.15° (Brewster angle = $\arctan n_{water}/n_{air}$, n being the refractive index), essentially no light is reflected. However, when a monolayer is present at the interface, light is reflected because the Brewster conditions are no longer fulfilled. The water surface then appears dark and the thin film lighter. The intensity of the reflected light is proportional to the thickness (d) and refractive index (n) of the film. The refractive indices of the *FnHm* diblocks (1.37 for *F*8*H*16, 1.38 for *F*8*H*18 and *F*8*H*20, and 1.36 for *F*10*H*16) were estimated with the equation $n = (1.26n + 1.43)/(n+m)$, 1.26 and 1.43 being the refractive indices for a fluorocarbon and a hydrocarbon, respectively.[56,57] A Bam2Plus microscope (NFT, Göttingen, Germany) equipped with a KSV Minitrough Langmuir system was used for the experiments. The compression speed was 1.5 $cm^2\,min^{-1}$ for capturing snapshots, and 3.75 $cm^2\,min^{-1}$ for film-thickness monitoring. The amounts of diblocks deposited were: 60 μL of a 2 $mmol\,L^{-1}$ solution of *F*8*H*20 for the snapshots of Figure 6a–f, isotherm, and thickness profile; 40 μL of a 2 $mmol\,L^{-1}$ solution of *F*10*H*16 for the snapshots of Figure 8Aa–e and Figure 8Ci–j′; 60 μL of the 2 $mmol\,L^{-1}$ solution for the snapshots of Figure 8Bf–h and Figure 8Dk,l; 40 or 60 μL of the 2 $mmol\,L^{-1}$ solution for the isotherm measurements; and 40 μL of a 4 $mmol\,L^{-1}$ solution for the thickness profile. Errors on the height measurements were estimated at ±1 or 2 nm, depending on the experiment.

Acknowledgements

The authors thank the Centre National de la Recherche Scientifique (CNRS) and the University of Strasbourg for financial support. C.d.G.L. acknowledges the CNRS and Région Alsace for a doctoral fellowship and GIS Fluor for a travel fellowship. Thanks to C. Contal (ICS, Strasbourg) for the AFM images.

[1] P. Metrangolo, G. Resnati, *Science* **2008**, *321*, 918–919.
[2] P. Metrangolo, F. Meyer, T. Pilati, G. Resnati, G. Terraneo, *Angew. Chem.* **2008**, *120*, 6206–6220; *Angew. Chem. Int. Ed.* **2008**, *47*, 6114–6127.
[3] H. Ringsdorf, B. Schlarb, J. Venzmer, *Angew. Chem.* **1988**, *100*, 117–162; *Angew. Chem. Int. Ed. Engl.* **1988**, *27*, 113–158.
[4] J. Gao, S. Qiao, G. M. Whitesides, *J. Med. Chem.* **1995**, *38*, 2292–2301.
[5] J. G. Riess, *Tetrahedron* **2002**, *58*, 4113–4131.
[6] M. P. Krafft, *J. Polym. Sci. Part A: Polym. Chem.* **2006**, *44*, 4251–4258.
[7] J. K. Montclare, D. A. Tirrell, *Angew. Chem.* **2006**, *118*, 4630–4633; *Angew. Chem. Int. Ed.* **2006**, *45*, 4518–4521.
[8] S. Marie Bertilla, J.-L. Thomas, P. Marie, M. P. Krafft, *Langmuir* **2004**, *20*, 3920–3924.
[9] Z. Li, E. Kesselman, Y. Talmon, M. A. Hillmyer, T. P. Lodge, *Science* **2004**, *306*, 98–101.
[10] S. Kubowicz, J.-F. Baussard, J.-F. Lutz, A. F. Thünemann, H. von Berlepsch, A. Laschewsky, *Angew. Chem.* **2005**, *117*, 5397–5400; *Angew. Chem. Int. Ed.* **2005**, *44*, 5262–5265.
[11] L. Nordstierna, I. Furo, P. Stilbs, *J. Am. Chem. Soc.* **2006**, *128*, 6704–6712.
[12] J. G. Riess, *J. Drug Targeting* **1994**, *2*, 455–468.
[13] B. P. Binks, P. D. I. Fletcher, W. F. C. Sager, R. L. Thompson, *Langmuir* **1995**, *11*, 977–983.
[14] W. Mahler, D. Guillon, A. Skoulios, *Mol. Cryst. Liq. Cryst. Lett.* **1985**, *2*, 111–119.
[15] F. G. Tournilhac, P. Bassoul, R. Cortès, *Mol. Cryst. Liq. Cryst.* **2001**, *362*, 45–65.
[16] E. Sloutskin, H. Kraack, B. Ocko, J. Ellmann, M. Möller, P. Lo Nostro, M. Deutsch, *Langmuir* **2002**, *18*, 1963–1967.
[17] M. P. Turberg, J. E. Brady, *J. Am. Chem. Soc.* **1988**, *110*, 7797–7801.
[18] B. P. Binks, P. D. I. Fletcher, S. N. Kotsev, R. L. Thompson, *Langmuir* **1997**, *13*, 6669–6682.
[19] P. Lo Nostro, *Curr. Opin. Colloid Interface Sci.* **2003**, *8*, 223–226.
[20] M. P. Krafft, M. Goldmann, *Curr. Opin. Colloid Interface Sci.* **2003**, *8*, 243–250.
[21] M. Schmutz, B. Michels, P. Marie, M. P. Krafft, *Langmuir* **2003**, *19*, 4889–4894.
[22] F. Gerber, M. P. Krafft, T. F. Vandamme, M. Goldmann, P. Fontaine, *Biophys. J.* **2006**, *90*, 3184–3192.
[23] C.-Y. Ku, P. Lo Nostro, S.-H. Chen, *J. Phys. Chem. B* **1997**, *101*, 908–914.
[24] B. P. Binks, P. D. I. Fletcher, W. F. C. Sager, R. L. Thompson, *J. Mol. Liq.* **1997**, *72*, 177–190.
[25] G. L. Gaines, *Langmuir* **1991**, *7*, 3054–3056.
[26] Z. Huang, A. A. Acero, N. Lei, S. A. Rice, Z. Zhang, M. L. Schlossman, *J. Chem. Soc. Faraday Trans.* **1996**, *92*, 545–552.
[27] S. Wang, R. Lunn, M. P. Krafft, R. M. Leblanc, *Langmuir* **2000**, *16*, 2882–2886.
[28] M. P. Krafft, F. Giulieri, P. Fontaine, M. Goldmann, *Langmuir* **2001**, *17*, 6577–6584.
[29] M. Maaloum, P. Muller, M. P. Krafft, *Angew. Chem.* **2002**, *114*, 4507–4510; *Angew. Chem. Int. Ed.* **2002**, *41*, 4331–4334.
[30] G.-F. Zhang, P. Marie, M. Maaloum, P. Muller, N. Benoit, M. P. Krafft, *J. Am. Chem. Soc.* **2005**, *127*, 10412–10419.
[31] A. El Abed, M.-C. Fauré, E. Pouzet, O. Abillon, *Phys. Rev. E* **2002**, *65*, 051603.
[32] A. L. Simões Gamboa, E. Filipe, P. Brogueira, *Nano Lett.* **2002**, *2*, 1083–1086.
[33] A. Mourran, B. Tartsch, M. O. Gallyamov, S. Magonov, D. Lambreva, B. I. Ostrovskii, I. P. Dolbnya, W. H. de Jeu, M. Moeller, *Langmuir* **2005**, *21*, 2308–2316.
[34] M. Broniatowski, J. Minones, P. Dynarowicz-Latka, *J. Colloid Interface Sci.* **2004**, *279*, 552–558.
[35] M. Broniatowski, I. Sandez Macho, J. Minones, P. Dynarowicz-Latka, *Appl. Surf. Sci.* **2005**, *246*, 342–347.
[36] M. Broniatowski, N. V. Romeu, P. Dynarowicz-Latka, *J. Colloid Interface Sci.* **2008**, *325*, 464–471.
[37] M. O. Gallyamov, A. Mourran, B. Tartsch, R. A. Vinokur, L. N. Nikitin, A. R. Khokhlov, K. Schaumburg, M. Möller, *Phys. Chem. Chem. Phys.* **2006**, *8*, 2642–2649.
[38] M. P. Krafft, J. G. Riess, *Chem. Rev.* **2009**, *109*, 1714–1792.
[39] P. Fontaine, M. Goldmann, P. Muller, M.-C. Fauré, O. Konovalov, M. P. Krafft, *J. Am. Chem. Soc.* **2005**, *127*, 512–513.
[40] G. Zhang, M. Maaloum, P. Muller, N. Benoit, M. P. Krafft, *Phys. Chem. Chem. Phys.* **2004**, *6*, 1566–1569.
[41] A. Gonzàlez-Pérez, C. Contal, M. P. Krafft, *Soft Matter* **2007**, *3*, 191–193.
[42] A. N. Semenov, A. Gonzàlez-Pérez, M. P. Krafft, J.-F. Legrand, *Langmuir* **2006**, *22*, 8703–8717.
[43] A. R. Tao, J. Huang, P. Yang, *Acc. Chem. Res.* **2008**, *41*, 1662–1673.
[44] D. C. Tully, J. M. J. Fre'chet, *Chem. Commun.* **2001**, 1229–1239.
[45] H. E. Ries Jr. , *Nature* **1979**, *281*, 287–289.
[46] D. Vollhardt, M. Ziller, U. Retter, *Langmuir* **1993**, *9*, 3208–3211.
[47] K. S. Birdi, D. T. Vu, *Langmuir* **1994**, *10*, 623–625.
[48] A. Angelova, D. Vollhardt, R. J. Ionov, *J. Phys Chem.* **1996**, *100*, 10710–10720.
[49] K. Y. C. Lee, *Annu. Rev. Phys. Chem.* **2008**, *59*, 771–791.
[50] M. Broniatowski, N. Vila-Romeu, M. Nieto-Suarez, P. Dynarowicz-Latka, *J. Phys. Chem. B* **2007**, *111*, 12787–12794.
[51] P. Nitoń, A. Żywociński, R. Holyst, R. Kieffer, C. Tschierske, J. Paczesny, D. Pociecha, E. Górecka, *Chem. Commun.* **2010**, *46*, 1896–1898.
[52] S. Baoukina, L. Monticelli, H. J. Risselada, S. J. Marrink, D. P. Tieleman, *Proc. Natl. Acad. Sci. USA* **2008**, *105*, 10803–10808.
[53] O. Gang, J. Ellmann, M. Möller, H. Kraak, E. B. Sirota, B. M. Ocko, M. Deutsch, *Europhys. Lett.* **2000**, *49*, 761–767.
[54] P. Marczuk, P. Lang, G. H. Findenegg, S. K. Mehta, M. Möller, *Langmuir* **2002**, *18*, 6830–6838.
[55] N. O. Brace, *J. Org. Chem.* **1962**, *27*, 3033–3038.
[56] Phys. Chem. Suite, version 12.0, Advanced Chemistry Development (ACD Inc., Toronto, ON, Canada), **2009**, http://www.acdlabs.com.
[57] *Handbook of Chemistry and Physics*, 77th ed. (Ed.: D. R. Lide), CRC Press, New York, **1996–1997**.

Received: December 23, 2009
Published online: May 12, 2010

